ELSEVIER

International Journal of Mass Spectrometry 219 (2002) 189–201

International Journal of Mass Spectrometry

www.elsevier.com/locate/ijms

Fragmentation energetics of small peptides from multiple-collision activation and surface-induced dissociation in FT-ICR MS

Julia Laskin*, Eduard Denisov, Jean H. Futrell

Pacific Northwest National Laboratory, William R. Wiley Environmental Molecular Sciences Laboratory, P.O. Box 999 (K8-96), Richland, WA 99352, USA

Received 26 June 2001; accepted 3 October 2001

Abstract

Multiple-collision activation (MCA-CID) using the sustained off-resonance irradiation (SORI) method and surface-induced dissociation (SID) of protonated tri- and tetraalanine $(AAA)H^+$ and $(AAAA)H^+$ were investigated using a 7 T Fourier Transform Ion Cyclotron Resonance Mass Spectrometer (FT-ICR MS). Energy-resolved fragmentation efficiency curves (FECs) obtained using both activation techniques were modeled using RRKM/QET formalism. Comparison of rates of formation of fragment ions originating from C- and N-terminal dissociation of protonated tetraalanine as a function of collision energy demonstrates that threshold energies for these dissociation channels are identical and that entropic factors are very similar. For tetraalanine modeling of both SID and MCA-CID experimental results provides reliable values for dissociation thresholds for the principal dissociation channels. However, this is not the case for protonated trialanine, where C-terminal fragmentation is preferred entropically but has higher dissociation energy and a slower rate over the range of collision energies investigated. Dissociation thresholds for the formation of y ions extracted from MCA-CID data for trialanine were substantially higher than thresholds obtained from SID data. Because our modeling approach assumes instantaneous ion activation, this difference is attributed to the slow nature of MCA-CID that becomes apparent for competing reactions with a substantial difference between dissociation thresholds. In this case, fragmentation via a higher-energy channel competes with stepwise ion activation. Consequently, MCA-CID results in effective discrimination against higher activation energy fragmentation pathways. For the series di-, tri-, and tetraalanine the lowest energy dissociation channels have thermochemical thresholds of 2.11, 1.46 and 1.20 eV, respectively based on our SID results. This demonstrates that thermochemical stability decreases with increasing size of the peptide. (Int J Mass Spectrom 219 (2002) 189–201)

Keywords: Multiple-collision activation; Surface-induced dissociation; SORI-CID; Protonated peptides; Fragmentation energetics

1. Introduction

In the last decade, tandem mass spectrometry (MS/MS) became an important tool for peptide sequencing, structure determination and investigation of dissociation mechanisms of biomolecules. Fragmentation patterns of peptides in a mass spectrometer are commonly used as fingerprints of their primary and secondary structure. The type and amount of fragments observed in the mass spectrum are controlled by the energetics and dynamics of fragmentation, the internal energy distribution of excited ions, and

* Corresponding author. E-mail: julia.laskin@pnl.gov

1387-3806/02/$ – see front matter
PII S1387-3806(01)00582-6

the instrumental time-window. Knowledge of peptide fragmentation energetics and mechanisms as well as understanding of the energy deposition in the ion activation process constitutes a basis for interpreting and predicting the MS/MS spectra of peptides.

Mechanisms of peptide fragmentation have been recently reviewed [1–4]. The so-called sequence-specific fragments that result from bond cleavages along peptide backbone commonly dominate mass spectra of protonated peptides. Cleavage of peptide (amide) bonds results in formation of **b** and **y** ions if the charge remains on the N- or C-terminus, respectively. It has been suggested that **b** ions are protonated oxazolones whereas **y** ions are eliminated as protonated linear peptides or amino acids [5,6]. Loss of CO from **b** ions gives rise to a series of **a** ions. Losses of NH_3 and H_2O from the molecular ion and from **b** and **y** fragments are also observed. Internal fragments and rearrangement products can substantially complicate peptide mass spectra. Depending on the primary and secondary structure of a particular peptide the propensity to form internal fragments can be very high. These fragmentation mechanisms are readily determined by multiple stages of MS analysis (MS^n).

MS/MS experiments involve mass selection of ions in the first MS stage, their subsequent excitation using any of ion activation techniques followed by the detection of the product-ion mass spectrum. It follows that ion activation is a crucial step in MS/MS studies. Multiple-collision activation [7] (MCA-CID) is, one of the most widely used ion activation methods. It is conveniently implemented in ion traps and involves relatively slow excitation of the precursor ion by absorption of small amounts of internal energy in multiple collisions with neutral gas. Surface-induced dissociation [8] (SID) is a feasible alternative to MCA-CID. In contrast to MCA-CID ion-surface collision results in a very fast excitation of precursor ions. We have recently compared these two ion activation techniques by conducting collision energy-resolved experiments of a series of small alanine-containing peptides in a Fourier transform ion cyclotron resonance mass spectrometer (FT-ICR MS) [9]. The comparative study suggested that MCA-CID and normal-incidence ion-surface impact with fluorinated self-assembled monolayer (SAM) surface produce internally excited ions with very similar quasithermal distributions of internal energies.

In addition to qualitative comparison between the MCA-CID and SID experimental results we can model the collision energy-resolved fragmentation efficiency curves (FECs) to extract dissociation energies for different reaction channels. This is done using a modeling approach developed by us recently [10,11] where FECs are reconstructed using RRKM theory and a proposed analytical form for the internal energy deposition function (EDF) [10,11]. The method has been used to study fragmentation energetics of bromobenzene [10], 1-bromonaphthalene [11] radical cations and protonated dialanine [12]. Both multiple-collision CID and SID data could be modeled using the same strategy and the same analytical form for the EDF.

This study is a continuation of the on-going research in our laboratory focused on the energetics and mechanisms of peptide fragmentation. Here we present a detailed investigation of the energetics of fragmentation of protonated tri- and tetraalanine. Dissociation energies are extracted from the modeling of multiple-collision CID and SID experiments.

2. Experimental

Experiments were performed on the University of Delaware 7 T Bruker BioApex^{TM} FT-ICR Mass Spectrometer modified for SID studies. The system is operated at an indicated base pressure of 5×10^{-10} Torr. Tri- and tetraalanine were purchased from Sigma (St. Louis, MO) and used without further purification. Sample solutions (10–50 μM in 49.5:49.5:1, water–methanol–acetic acid solution) were infused into the ESI source using a Harvard Apparatus (Natick, MA) syringe pump at a flow rate of 20 μL/h.

Sustained off-resonance irradiation (SORI)-CID experiments were performed as described earlier [10]. Ions generated in an electrospray source are accumulated in a hexapole for a predefined trapping time that was approximately 1 s in these experiments. The ions

are extracted from the hexapole, transferred into the ICR cell by a series of ion transfer lenses and captured in the cell. Ions were trapped in the cell by applying a 2 V potential to the trapping plates. Excess kinetic energy was removed from the ions by pulsing Ar into the cell for a duration of about 300 ms at a maximum pressure of 2×10^{-6} Torr. Ions were allowed to cool to thermal equilibrium by radiative and collisional cooling during the pumping delay of 5 s. The precursor ion was then isolated using a correlated sweep procedure. A second Ar pulse was then introduced to remove any excess kinetic energy gained by the molecular ions during the isolation event. A third Ar pulse was introduced into the cell for collisional activation. Protonated molecules were radially excited slightly off-resonance ($\Delta f = -700$ Hz) for 100 ms at nearly fixed Ar pressure. It should be noted that ions are continuously accelerated/decelerated as they undergo collisions with Ar during the 100 ms SORI excitation event. The pressure calibration method described by us previously [10], was used throughout this work. The kinetic energy of the ions was increased by changing the peak-to-peak voltage applied to the excitation plates. After 5 s pumping delay the ions were excited by broadband chirp excitation for detection.

Double-resonance experiments combined with SORI excitation were performed by applying an additional 100 V_{p-p} rf wave simultaneously with the SORI excitation pulse with a frequency corresponding to the cyclotron frequency of the ion to be ejected. The ejecting pulse (typically 3 s) was chosen to be long enough to allow ejection of the ions formed both during the SORI excitation pulse and after the excitation wave has been switched off. Basic considerations for choosing RF amplitude of the ejection wave and possible reasons for incomplete ejection were discussed elsewhere [11].

Our experimental setup for SID experiments was described elsewhere [13]. Briefly, the surface was introduced into the ICR cell through the aperture in the rear ICR trapping plate at 90 °C to the magnetic field. The surface holder was in electrical contact with the back trapping plate. Ions produced in the ESI source were accumulated in the hexapole and extracted after a delay of 0.4 s by a 100 μs extraction pulse. The ions were then transferred into the ICR cell by a series of lenses. The ion's kinetic energy was varied by floating the hexapole rods, skimmer and hexapole extraction plate. The SID collision energy was determined as the difference between the source offset and the target potentials. Slightly asymmetric potential was created in the ICR cell by applying 5 V to the front trapping plate and 2 V to the rear plate and the surface. Secondary ions produced by surface impact are slightly accelerated towards the center of the cell and turned around by the 5 V potential applied to the front trapping plate. At this time dynamic voltage trapping (DVT) is activated by applying 7 V potential to both trapping plates. Delay time between the hexapole extraction and the activation of the DVT was chosen based on SIMION simulation of the ion's trajectories. The delay varied from 250 to 75 μs for trialanine and from 300 to 100 μs for tetraalanine when the collision energy was changed from 5 to 50 eV. After an additional delay of 1–3 s the ions were excited by broadband chirp for detection.

Self-assembled monolayers (SAMs) were prepared on a clean polycrystalline gold surface by immersing the surface holder in a 1 mM ethanol solution of the FC_{12} alkyl thiol ($CF_3(CF_2)_9C_2H_4SH$) for at least 24 h. Extra layers of the SAMs were removed by four-stage rinsing (10 min ultrasonic cleaning) of the assembly in ethanol.

FECs representing relative yields of different ions as a function of collision energy were constructed from the set of collision energy-resolved mass spectra. MCA-CID FECs are plotted as a function of the maximum center-of-mass (CM) collision energy. CID experiments presented in this study were conducted at two pressures corresponding to collision numbers (n) of 5 and 15 (hard-sphere collision cross sections of 105 and 115 $Å^2$ for $(AAA)H^+$ and $(AAAA)H^+$ collisions with Ar, respectively were estimated based on the ion mobility data [14]). We will refer to the experiment with $n = 5$ as low-pressure MCA-CID and to the experiment with $n = 15$ as high-pressure MCA-CID. The choice of CID parameters was dictated by the results of our previous studies, which demonstrated that fragmentation

efficiency upon MCA-CID is substantially enhanced when collision number increases from 3 to 15 [10,11]. However, further increase in pressure does not affect the fragmentation efficiency to a significant extent. This is probably a result of essential thermalization of the system at collision number of 15 and above. This conclusion is in agreement with the results of master equation modeling of the internal energy transfer in MCA-CID [15].

3. Results and discussion

3.1. Dissociation pathways

Fig. 1 shows representative mass spectra of tri- and tetraalanine obtained under high-pressure multiple-collision conditions ($n = 15$) and the maximum CM collision energy of 3 eV. Dominant fragments of protonated trialanine are $\mathbf{b_2}$, $\mathbf{a_2}$ and $\mathbf{a_1}$ ions. While these fragments are also abundant in the spectrum of tetraalanine, $\mathbf{y_2}$ ion is observed as the main fragment of $(AAAA)H^+$ over a wide range of collision energies.

Double-resonance experiments were performed to establish dissociation pathways of tri- and tetraalanine and their fragments. In these experiments, a selected fragment is continuously ejected from the ICR cell during the SORI excitation. The ejecting rf wave is continued for three additional seconds after the SORI excitation pulse is turned off to ensure a complete ejection of all the ions of the selected mass-to-charge ratio. As a result of ejection of a particular fragment ion, intensities of all the ions for which it is a precursor are strongly reduced. These experiments were performed with a SORI excitation voltage that corresponds to the maximum CM collision energy of 5 eV and Ar pressure corresponding to an average collision number of 15. Under these CID conditions all fragment ions of interest are present in a normal SORI-CID spectrum.

It should be noted that, in some cases double-resonance ejection could introduce some ambiguity into the determination of dissociation pathways of ions. Accurate double-resonance experiments require a compromise for the amplitude of the ejecting wave. The amplitude should be low enough to avoid translational off-resonance excitation of adjacent masses and high enough to ensure a complete and fast ejection of ions from the ICR cell while minimizing unimolecular or collision-induced decay of the precursor ion during ejection. In the present study, 100 V peak-to-peak voltage was employed. Under these conditions the ejection time in our system is about 0.5 ms. It follows that any fragmentation that is faster than 0.5 ms can contribute to the observed "incomplete ejection" of fragment ions.

Taking the above considerations into account the results of double-resonance experiments summarized

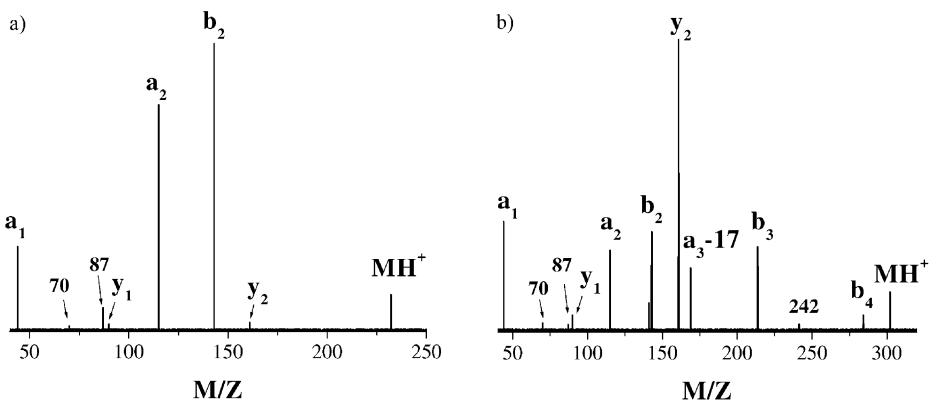

Fig. 1. Representative mass spectra of (a) $(AAA)H^+$ and (b) $(AAAA)H^+$ obtained under high-pressure multiple collision conditions at maximum CM energy of 3 eV.

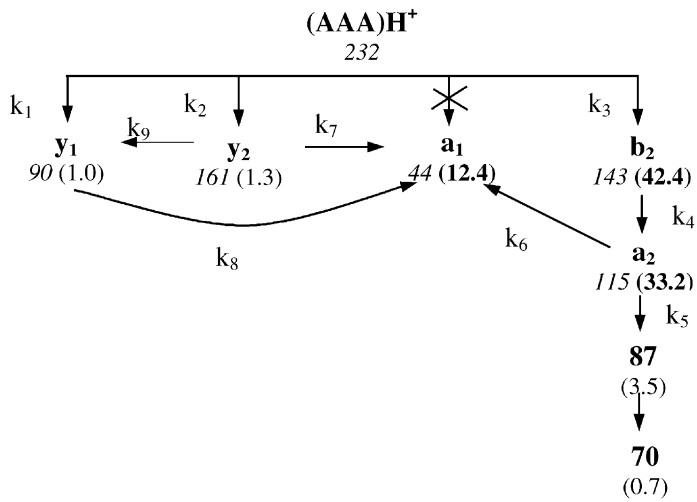

Scheme 1. Reaction scheme for $(AAA)H^+$. Mass-to-charge ratios are shown in italics and relative abundances of fragment ions in parentheses. (The abundances are obtained from the high-pressure MCA-CID experiment at 3 eV CM energy.)

in Schemes 1 and 2 were critically evaluated. For example, formation of the immonium ion ($\mathbf{a_1}$) directly from $(AAA)H^+$ could not be ruled out based on the double-resonance ejection. However, RRKM modeling (discussed in Section 3.2) demonstrated that this reaction pathway does not compete with the formation of the $\mathbf{b_2}$ and $\mathbf{y_2}$ ions from the protonated precursor ion. Specifically, substantially higher

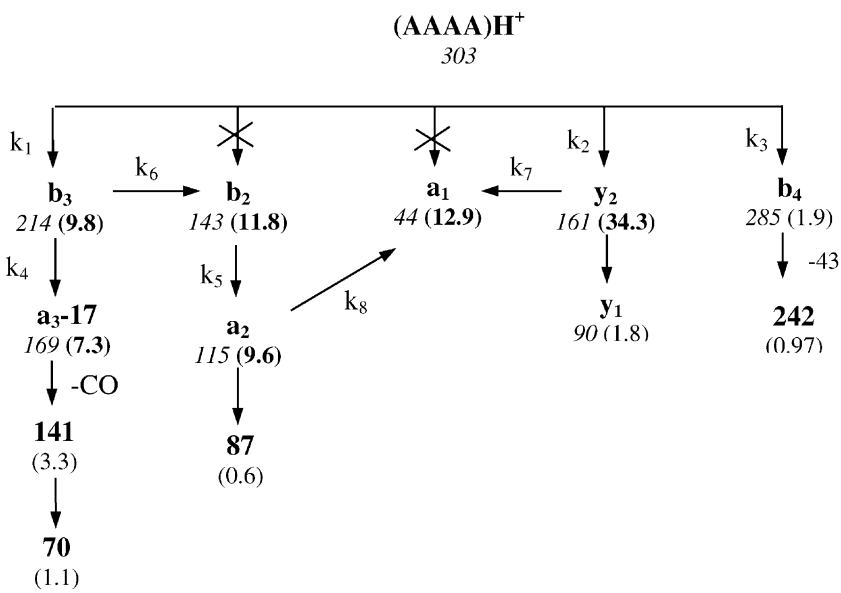

Scheme 2. Reaction scheme for $(AAAA)H^+$. Mass-to-charge ratios are shown in italics and relative abundances of fragment ions are in parentheses.

appearance energy for this reaction channel was observed experimentally. Similar results were obtained for the $\mathbf{b_2}$ and $\mathbf{a_1}$ ions that could possibly originate from $(AAAA)H^+$. These reactions are marked by cross signs in Schemes 1 and 2.

Close examination of Schemes 1 and 2 reveals some similarities and differences between the fragmentation pathways of tri- and tetraalanine. One of the dominant dissociation channels for both ions is the formation of $\mathbf{b_{n-1}}$ ion, i.e., the N-terminal fragment that contains one less amino acid residues than the corresponding precursor ion. The $\mathbf{b_2}$ ion formation from trialanine is accompanied by the formation of the complementary $\mathbf{y_1}$ ion. However, this is not the case for $(AAAA)H^+$ fragmentation, where the $\mathbf{y_1}$ ion (complementary to the $\mathbf{b_3}$ ion) is not formed from MH^+. It is accepted that N-terminal fragments (**b** ions) produced from small peptides have protonated oxazolone structure (I) whereas C-terminal fragments (**y** ions) are eliminated as protonated linear peptides and/or amino acids [16,17]. Wesdemiotis and co-workers have demonstrated that proton affinity of small oxazolone giving rise to the $\mathbf{b_2}$ ion is higher than proton affinity of the amino acid ($\mathbf{y_1}$ ion) [1]. As a result of a competition for the charge between these two fragments, the fragment with higher proton affinity (the $\mathbf{b_2}$ ion) is preferentially formed. It follows that the difference in relative intensities of the $\mathbf{b_2}$ and $\mathbf{y_1}$ ions from $(AAA)H^+$ (Scheme 1) can be rationalized by the difference in proton affinities. The $\mathbf{b_3}$ fragment of $(AAAA)H^+$ is expected to be even more basic than the $\mathbf{b_2}$ ion. It is not surprising that the reaction $(AAAA)H^+ \rightarrow \mathbf{y_1}$ is not observed.

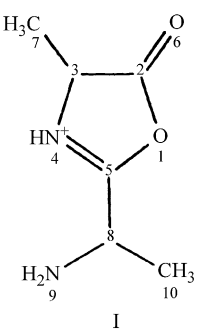

I

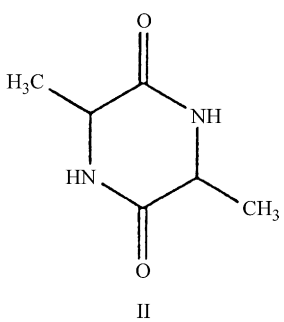

II

The $\mathbf{y_2}$ fragment of tetraalanine (Scheme 2) is also produced without the complementary $\mathbf{b_2}$ ion. This indicates that for this reaction channel the formation of neutral diketopiperazine (II) and protonated dipeptide is favored over the formation of protonated oxazolone (I) and neutral dipeptide (Scheme 7 in [1]). Based on thermochemical information [18] we estimate that the relative energies of formation of these two pairs differ by about 10 kcal/mol strongly favoring formation of $\mathbf{y_2}$ ion.[1]

Interesting trends are also observed in the secondary fragmentation channels of tri- and tetraalanine. The $\mathbf{b_2}$ ion undergoes normal fragmentation by loss of CO to yield the $\mathbf{a_2}$ ion [16]. In contrast, no $\mathbf{a_3}$ ions have been observed in mass spectra of tetraalanine at all collision energies. Instead, dissociation of $\mathbf{b_3}$ ion results in the formation of $\mathbf{a_3}$-17 fragment. Accurate mass measurement confirmed that the loss of CO in this case occurs simultaneously with the loss of NH_3. An abundant $\mathbf{a_3}$-17 fragment was previously observed in high-energy CID studies of polyalanines, [16] however, the $\mathbf{a_3}$ ion was also formed in the high-energy collisional activation. This indicates that the formation of $\mathbf{a_3}$ ions requires high internal excitation. The proton located on N4 (I) facilitates the loss of CO from protonated oxazolone. It has been shown that the C_2–O_1 bond is substantially weakened in protonated oxazolone as compared to its neutral structure [18]. However, if the proton is remote from the ring nitrogen (N4) opening of the ring requires higher-energy and becomes unfavorable. In the $\mathbf{b_3}$ ion protonation can occur on the amino nitrogen and interaction of the terminal NH_3^+ with the oxazolone ring facilitates the loss of CO and NH_3 from the $\mathbf{b_3}$ ion.

3.2. RRKM modeling

3.2.1. Modeling approach

RRKM modeling approach employed in this work was described in detail elsewhere [10–12]. Energy

[1] It should be noted that termochemical data are available only for the fragments of polyglycines. However, it is reasonable to expect only a small difference in the thermochemistry of small polyglycines and polyalanines.

dependent microcanonical rate constants for the major reaction channels were calculated using RRKM/QET. Fragmentation probability as a function of the internal energy of the parent ion and the experimental observation time (t_r), $F(E, t_r)$, was calculated from the rate-energy $k(E)$ dependencies. The EDF was described by the following analytical expression:

$$P(E, E_{coll}) = \frac{(E - \Delta)^l \exp(-(E - \Delta)/g(E_{coll}))}{C} \quad (1)$$

where l and Δ are parameters, $C = \Gamma(l + 1)[g(E_{coll})]^{l+1}$ is a normalization factor and $g(E_{coll})$ has the form:

$$g(E_{coll}) = A_2 E_{CM}^2 + A_1 E_{CM} + A_0 \quad (2)$$

where A_0, A_1 and A_2 are parameters. For MCA-CID results A_0 was replaced with $E_{th}/(l+1)$, where E_{th} is the average thermal energy of protonated dialanine at 298 K [11,12]. E_{coll} equals the collision energy for SID experiments and the maximum CM collision energy for MCA-CID experiments.

The normalized signal intensity for a particular reaction channel is given by the equation:

$$I_i(E_{coll}) = \int_0^\infty F_i(E, t) P(E, E_{coll})\, dE \quad (3)$$

Calculated FECs were constructed from the energy-dependent signal intensities for the precursor ion and its fragments. The results were compared to the experimental FECs and the fitting parameters varied until the best fit to experimental FECs was obtained. The fitting parameters included critical energies of the reaction channels indicated by the rate constant signs in Schemes 1 and 2, activation entropies for some of these reactions, plus parameters characterizing the EDF (Eqs. (1) and (2)). RRKM parameters obtained for several reaction channels studied in our previous work [12] were incorporated in the modeling. However, these parameters were allowed to vary in order to check correlation between our previous results and the results of the present study. The same approach was used to model the FECs obtained in MCA-CID and SID experiments. Reaction times of 5 and 3 s were used to model MCA-CID and SID results, respectively.

3.2.2. RRKM parameters

Vibrational frequencies of protonated precursor ions and their fragments were estimated using AM1 calculations. Because RRKM calculations are not sensitive to the details of vibrational frequencies of the precursor ion and transition states but rather to the relative changes in frequencies along the reaction coordinate a more elaborate modeling of vibrational frequencies is unnecessary in the present investigation. Vibrational frequencies of transition states were estimated as follows: one frequency in the range of 1000–1500 cm^{-1}, corresponding to C–N, C–O or C–C stretch (depending on the reaction), was chosen as the relevant reaction coordinate and eight other frequencies in the range 300–1500 cm^{-1} were varied to obtain the best fit with experimental data. This allowed us to vary activation entropy ($\Delta S^{\ddagger}$) of any reaction channel over a very wide range. The internal energy of fragment ions was corrected for the energy partitioning between the ionic and neutral fragments as described elsewhere [11,12].

We have previously discussed the sensitivity of the RRKM modeling to different parameters [11,12]. For competing reaction channels the modeling is sensitive to both dissociation energies and activation entropies of all competing reactions. However, FECs for reaction channels which are not in competition with other reactions depend only on the critical energy for this particular reaction channel.

3.3. Fragmentation energetics and dynamics

Experimental FECs are compared with modeling results in Figs. 2 and 3. Fig. 2 shows FECs for $(AAA)H^+$ activated by ion-surface impact, while MCA-CID results for $(AAAA)H^+$ are summarized in Fig. 3. Similar quality fits (not shown) were obtained for other data acquired for low- and high-pressure MCA-CID and SID. To test uniqueness of the fits critical energies of one of the primary reactions for tri- and tetraalanine were systematically changed in increments of 0.02 eV and the rest of the fitting parameters were adjusted to

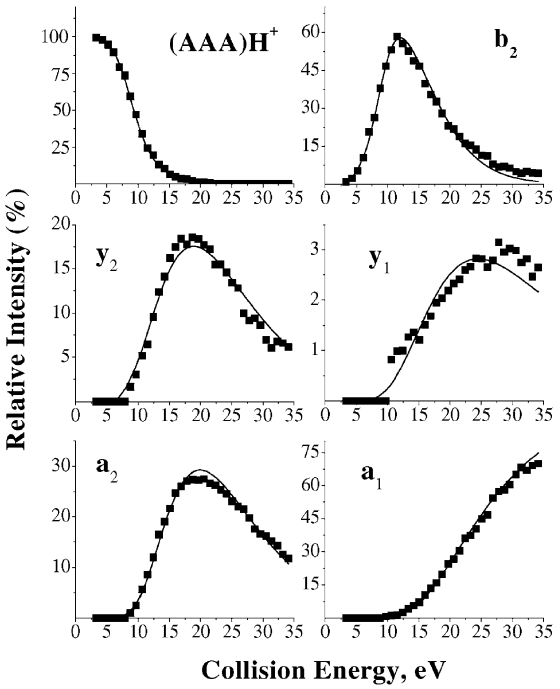

Fig. 2. Experimental and calculated SID FECs for the parent and major fragment ions of $(AAA)H^+$.

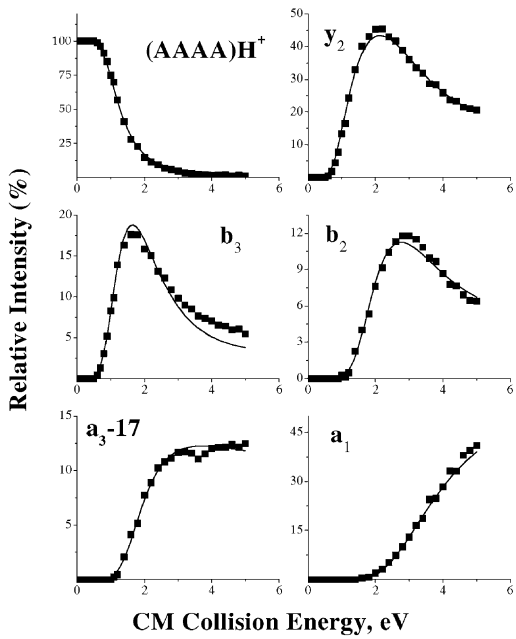

Fig. 3. Experimental and calculated MCA-CID FECs for the parent and major fragment ions of $(AAAA)H^+$.

give the best fit. This test revealed that the fits were unique within the error limits given in Tables 1 and 2.

3.3.1. Primary fragmentation of $(AAA)H^+$

Table 1 shows the activation parameters obtained for the three primary reaction channels for $(AAA)H^+$ from the modeling of low- (average collision number $n = 5$) and high-pressure ($n = 15$) MCA-CID and SID experiments. Although, there is a good agreement between the critical energies for the formation of the $\mathbf{b_2}$ ion from the protonated peptide (reaction 3), critical energies for reactions 1 and 2 from MCA-CID experiments are strongly overestimated. We have recently demonstrated that this difference can be attributed to the difference between the fast and slow ion activation [9]. When two competing reactions have substantially different dissociation energies, MCA-CID is in competition with fragmentation via the lowest-energy reaction channel. This results in effective discrimination against the high-energy channel and lower ion yields for this channel in MCA-CID mass spectra. Moreover, the appearance energy for the high-energy reaction channel is higher in MCA-CID because of the competitive shift introduced by the competition between ion activation and dissociation through this channel. Consequently, the modeling that assumes instantaneous deposition of internal energy into the precursor ion indicates higher dissociation threshold for the reaction channel affected by this type of discrimination.

To facilitate the discussion Fig. 4 shows the comparison between MCA-CID and SID results for $\mathbf{b_2}$, $\mathbf{y_2}$ and $\mathbf{y_1}$ ions. It is clear that relative intensities of y ions are suppressed in MCA-CID. However, the degree of discrimination is different for $\mathbf{y_2}$ and $\mathbf{y_1}$ ions. MCA-CID and SID intensities differ by a factor of 2.5 for the $\mathbf{y_1}$ ion and a factor of 12 for the $\mathbf{y_2}$ ion. The degree of discrimination depends on the relative critical energies for competing reactions. It follows that reaction 1: $(AAA)H^+ \rightarrow \mathbf{y_1}$ should be characterized by a lower critical energy than reaction 2: $(AAA)H^+ \rightarrow \mathbf{y_2}$. This surmise is confirmed by the modeling results

Table 1
RRKM/QET parameters for the primary reaction channels of $(AAA)H^+$

Experiment	Reaction	1 $MH^+ \rightarrow y_1$	2 $MH^+ \rightarrow y_2$	3 $MH^+ \rightarrow b_2$
MCA-CID ($n = 5$)[a]	E_0 (eV), $\Delta S^{\ddagger}$ (e.u.)[b]	1.76 (0.05)[c], 4.8 (0.5)	1.84 (0.04), 11.7 (1.5)	1.46 (0.04), 4.4 (0.5)
MCA-CID ($n = 15$)[a]	E_0 (eV), $\Delta S^{\ddagger}$ (e.u.)	1.72 (0.04), 4.5 (0.5)	1.86 (0.08), 11.9 (1.5)	1.42 (0.04), 4.8 (0.5)
SID	E_0 (eV), $\Delta S^{\ddagger}$ (e.u.)	1.59 (0.07)[d], 2.5 (1.5)	1.67 (0.05), 12.2 (1.5)	1.46 (0.05), 6.3 (0.8)

[a]These numbers denote the average number of collisions in the low-pressure ($n = 5$) and high-pressure ($n = 15$) MCA-CID experiments.
[b]Entropy unit (e.u.) = cal/(mol K).
[c]Uncertainties shown in parentheses were determined from the sensitivity analysis described in the text.
[d]Underlined are the suggested dissociation energies for these reactions (see text for discussion).

Table 2
RRKM/QET parameters for the primary reaction channels of $(AAAA)H^+$

Experiment	Reaction	1 $MH^+ \rightarrow b_3$	2 $MH^+ \rightarrow y_2$	3 $MH^+ \rightarrow b_4$
MCA-CID ($n = 5$)	E_0 (eV), $\Delta S^{\ddagger}$ (e.u.)[b]	1.25 (0.05)[a], 12.8 (1.0)	1.19 (0.04), 9.9 (0.3)	1.14 (0.04), −4.9 (0.7)
MCA-CID ($n = 15$)	E_0 (eV), $\Delta S^{\ddagger}$ (e.u.)	1.26 (0.05), 12.0 (0.3)	1.23 (0.03), 10.2 (0.5)	1.16 (0.04), −4.4 (0.5)
SID	E_0 (eV), $\Delta S^{\ddagger}$ (e.u.)	1.20 (0.06), 12.9 (0.3)	1.17 (0.05), 9.1 (0.3)	1.16 (0.05), −5.4 (0.5)
Average	E_0 (eV), $\Delta S^{\ddagger}$ (e.u.)	1.24 (0.06), 12.6 (1.1)	1.20 (0.05), 9.7 (1.2)	1.15 (0.05), −4.9 (0.8)

[a]Uncertainties shown in parentheses were determined from the sensitivity analysis described in the text.
[b]Entropy unit (e.u.) = cal/(mol K).

obtained from SID data (Table 1, underlined values), which indicate that the critical energy for reaction 1 is lower than the critical energy for reaction 2.

It is apparent that dissociation parameters obtained for $(AAA)H^+$ from MCA-CID curves using our modeling approach are not reliable. The proposed modeling is based on the assumption that the internal energy is instantly deposited in the parent ion in both MCA-CID and SID. However, this type of modeling is not applicable in the case when ion activation and dissociation are in a competition. Comparison between the SID and MCA-CID results suggests that the formation of $\mathbf{y_2}$ and $\mathbf{y_1}$ ions from $(AAA)H^+$ competes with the parent ion excitation. From the above discussion it follows that reliable information on the fragmentation energetics of trialanine can be obtained only from SID data.

The suggested values for critical energies and activation entropies are underlined in Table 1. With its dissociation threshold of 1.46 eV $\mathbf{b_2}$ ion formation is

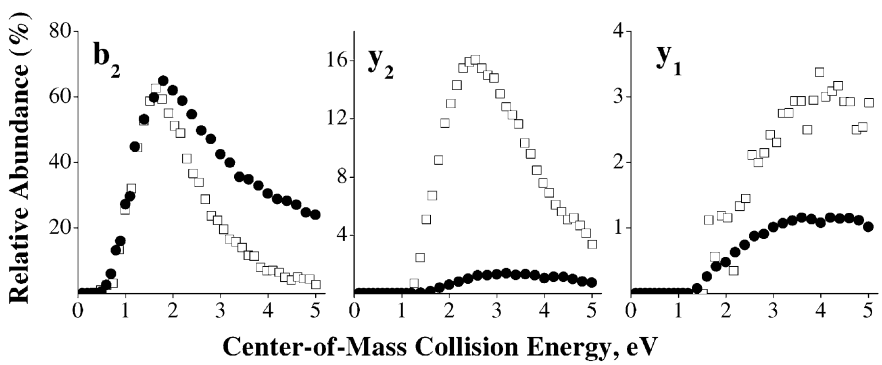

Fig. 4. Comparison between the high-pressure ($n = 15$) CID (filled circles) and SID (open squares) results for the three primary fragments of $(AAA)H^+$ (see [9] for details).

the lowest-energy reaction channel for protonated trialanine. The next reaction channel (formation of the $\mathbf{y_1}$ ion) requires 0.13 eV more energy and is characterized by a somewhat tighter transition state. This is manifested by the low abundance of the $\mathbf{y_1}$ ion even at high collision energies. In contrast, reaction 2 (formation of the $\mathbf{y_2}$ ion) that has the highest dissociation threshold (1.67 eV) competes very efficiently with reaction 3 at high energies because it proceeds via a very loose transition state.

3.3.2. Primary fragmentation of (AAAA)H^+

Dissociation parameters for the primary reaction channels of (AAAA)H^+ are summarized in Table 2. In this case there is a remarkable agreement between the dissociation energetics and dynamics obtained from MCA-CID and SID data. These results represent average values for the MCA-CID and SID experiments. As expected, rate constants for the formation of $\mathbf{y_2}$ and $\mathbf{b_3}$ ions are very similar. These reactions have the same critical energies within the experimental error and both proceed via very loose transition states. However, the loss of H_2O (reaction 3) requires substantial rearrangements and is characterized by a tight transition state. Previous studies, using H/D exchange suggested that "putative" **b** ions formed by the loss of water molecule from protonated polyglycines do not have an oxazolone structure [19]. Reid et al. observed that the putative $\mathbf{b_4}$ ion from protonated tetraglycine loses $NH{=}CH_2$ upon collisional activation [19]. It is interesting to note that the putative $\mathbf{b_4}$ ion from (AAAA)H^+ fragments very similarly via a loss of $NH{=}CH{-}CH_3$ (Scheme 2).

In summary, the thermochemical stability of small polyalanines studied so far decreases smoothly with increasing number of amino acid residues. The major channel for (AA)H^+ fragmentation requires 2.11 eV [12], whereas tri- and tetraalanine require 1.46 and 1.20 eV, respectively. This can be attributed to the increasing flexibility of the peptide backbone for larger peptides that makes nucleophile-electrophile interactions more accessible and thereby promotes fragmentation. Wysocki and co-workers obtained qualitatively similar results by examining the total rate of disappearance of protonated peptides using SID [20]. Very loose transition states for most of the primary reaction channels are indicative of the reaction pathways that involve fragmentation of ion-molecule complexes in the last rate determining stage of the reaction. This is in agreement with both experimental [21] and theoretical predictions [22].

3.3.3. Secondary fragmentation of small polyalanines

Energetics of secondary reactions from different precursor ions are summarized in Table 3. It is remarkable that in most cases our modeling provides very consistent results. Critical energies for reactions 1, 3 and 4 (Table 3) observed from different precursor ions demonstrate excellent agreement within the error bars. However, higher dissociation energy for the CO loss from the b_2 ion is obtained when the precursor ion

Table 3
The energetics of secondary reactions

Reaction	(AA)H^+ [a]	(AAA)H^+ [b]	(AAAA)H^+ [b]
(1) (AA)$H^+ \rightarrow a_1$	2.11 (0.15)[c]	2.00 (0.1)	2.15 (0.08)
(2) $b_2 \rightarrow a_2$	0.98 (0.07)	1.3 (0.05)	1.00 (0.05)
(3) $a_2 \rightarrow a_1$	0.97 (0.07)	0.92 (0.06)	0.95 (0.03)
(4) $y_1 \rightarrow a_1$	1.67 (0.35)	1.75 (0.1)	
(5) $b_3 \rightarrow b_2$			1.59 (0.05)
(6) $b_3 \rightarrow a_3$-17			1.53 (0.05)

[a] [9].
[b] This work.
[c] Uncertainties shown in parentheses were determined from the sensitivity analysis described in the text.

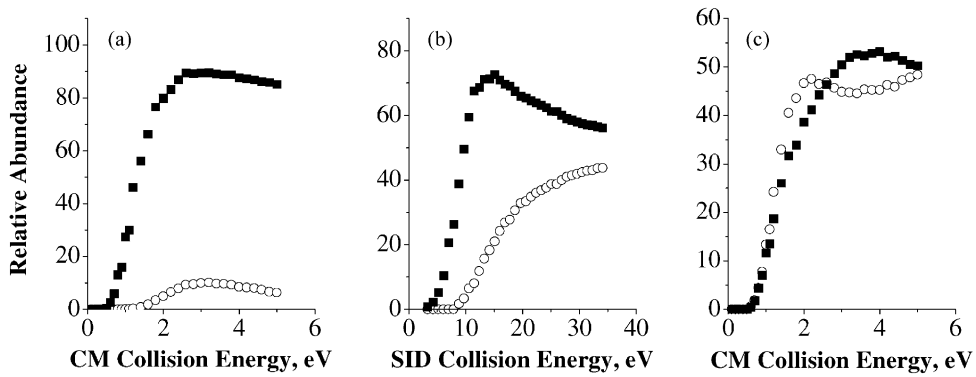

Fig. 5. Relative abundances of C-terminal (open circles) and N-terminal (filled squares) fragments originating from (a) $(AAA)H^+$ activated by multiple collisions with Ar (MCA-CID), (b) $(AAA)H^+$ activated by surface impact (SID) and (c) $(AAAA)H^+$ activated by multiple collisions with Ar (MCA-CID).

is $(AAA)H^+$. Using a lower threshold for this reaction resulted in a very poor modeling of the $(AAA)H^+$ data. The high critical energy could, in principle, indicate a different structure of the $\mathbf{b_2}$ ion originating from $(AAA)H^+$.

Very similar critical energies were obtained for reactions 5 and 6 (Table 3). Interestingly, formation of $\mathbf{b_2}$ ion from the $\mathbf{b_3}$ ion requires approximately 0.5 eV higher-energy than the loss of CO from the $\mathbf{b_2}$ ion. As mentioned earlier, if the proton in the $\mathbf{b_3}$ ion is not located on the oxazolone ring, the ring opening becomes unlikely and higher-energy reaction channels can open. Loss of CO and ammonia from the $\mathbf{b_3}$ ion confirms that in this ion the proton is located on the amine nitrogen.

3.4. C- and N-terminal fragments

Fig. 5(a–c) reports relative amounts of C- and N-terminal fragments from tri- and tetraalanine as a function of collision energy. It should be mentioned that the immonium ion ($\mathbf{a_1}$) originates from both C- and N-termini. Partitioning of $\mathbf{a_1}$ ion between C- and N-terminal fragmentation is shown in Fig. 6. It was extracted from the modeling by blocking the corresponding secondary reaction channels. For example, reactions 7 and 8 (Scheme 1) were blocked to determine the amount of $\mathbf{a_1}$ ions originating from the N-terminal fragments of $(AAA)H^+$. FECs for the $\mathbf{a_1}$ ion were appropriately divided between the C- and N-terminal fragments.

Fig. 5a and b summarize the relative yields of C- and N-terminal fragments from protonated trialanine obtained using MCA-CID and SID, respectively. It is clear that there is a dramatic difference between the SID and MCA-CID results. This can be rationalized by our earlier discussion on the discrimination against higher-energy reaction channels by MCA-CID

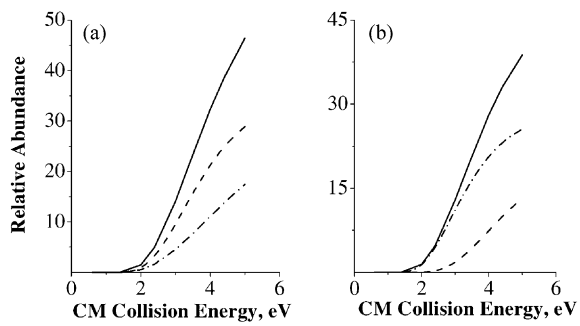

Fig. 6. Partitioning of $\mathbf{a_1}$ ion between C- and N-terminal fragmentation extracted from the modeling of high-pressure MCA-CID data for (a) $(AAA)H^+$, (b) $(AAAA)H^+$. Solid, dashed and dashed–dotted lines represent the overall amount of $\mathbf{a_1}$ ion, the amount of $\mathbf{a_1}$ produced from N-terminal fragments, and the amount of $\mathbf{a_1}$ produced from C-terminal fragments, respectively.

experiments. As shown in Fig. 5b, the threshold for the formation of C-terminal fragments is higher than the threshold for the formation of N-terminal fragments. At high collision energies the competition between these two reaction channels becomes important. In contrast, Fig. 5c indicates that both the energetics and dynamics for the formation of C- and N-terminal fragments from $(AAAA)H^+$ in MCA-CID are very similar. Consequently, these fragment ions are produced in the same proportion (approximately 1:1) over a wide range of energies. Similar results (not shown) were obtained for the SID fragments of protonated tetraalanine.

4. Summary

In this work, collision energy-resolved experiments were combined with RRKM-based modeling to study fragmentation energetics of protonated tri- and tetraalanine. Investigation of the primary reaction channels revealed that the thermochemical stability of small polyalanines decreases with increasing peptide size. Furthermore, we found that formation of C-terminal fragments from $(AAA)H^+$ is energetically more demanding than formation of N-terminal fragments. In contrast, both the energetics and dynamics of C- and N-terminal ion formation from $(AAAA)H^+$ are very similar. Dissociation energies of secondary reactions from different precursor ions are remarkably consistent suggesting the consistency of the modeling.

This work provides a further support for the utility of the modeling approach proposed by us recently for studying dissociation energetics and dynamics of large molecules [10,11]. However, the cross-correlation between the MCA-CID and SID data revealed that in some cases MCA-CID leads to effective discrimination against high-energy reaction channels. This occurs when the dissociation step competes with the ion activation step. As a result, the relative intensity of the $\mathbf{y_1}$ and $\mathbf{y_2}$ ions originating from $(AAA)H^+$ were suppressed in the multiple-collision experiment. We have demonstrated that in this case modeling of the collision energy-resolved MCA-CID data strongly overestimated critical energies for these reaction channels. Reliable energetics could be extracted only from the SID data.

Acknowledgements

This research was partially supported by NSF grants CHE-9616711 and CHE-9634238 and by DOE grant DE-FG02-97ER14813. Part of this research was conducted under the auspices of the Office of Basic Energy Sciences, US Department of Energy, under Contract DE-AC06-76RLO 1830 with the Battelle Memorial Institute, which operates the Pacific Northwest National Laboratory, a multi-program national laboratory operated from the Department of Energy.

References

[1] M.J. Polce, D. Ren, C. Wesdemiotis, J. Mass Spectrom. 35 (2000) 1391.
[2] V.H. Wysocki, G. Tsaprailis, L.L. Smith, L.A. Breci, J. Mass Spectrom. 35 (2000) 1399.
[3] A. Schlosser, W.D. Lehmann, J. Mass Spectrom. 35 (2000) 1382.
[4] R.A.J. O'Hair, J. Mass Spectrom. 35 (2000) 1377.
[5] T. Yalcin, I.G. Csizmadia, M.R. Peterson, A.G. Harrison, J. Am. Soc. Mass Spectrom. 7 (1996) 233.
[6] M.J. Nold, C. Wesdemiotis, T. Yalcin, A.G. Harrison, Int. J. Mass Spectrom. Ion Processes 164 (1997) 137.
[7] S.A. McLuckey, D.E. Goeringer, J. Mass Spectrom. 32 (1997) 461.
[8] R.G. Cooks, T. Ast, A. Mabud, Int. J. Mass Spectrom. Ion Processes 100 (1990) 209.
[9] J. Laskin, E. Denisov, J.H. Futrell, J. Phys. Chem. B 105 (2001) 1895.
[10] J. Laskin, M. Byrd, J.H. Futrell, Int. J. Mass Spectrom. 195/196 (2000) 285.
[11] J. Laskin, J.H. Futrell, J. Phys. Chem. A 104 (2000) 5484.
[12] J. Laskin, E. Denisov, J.H. Futrell, J. Am. Chem. Soc. 122 (2000) 9703.
[13] V.S. Rakov, J.H. Futrell, E.V. Denisov, D.P. Ridge, Eur. Mass Spectrom. 6 (2000) 299.
[14] R.R. Hudgins, Y. Mao, M.A. Ratner, M.F. Jarrold, Biophys. J. 76 (1999) 1591.
[15] J. Laskin, J.H. Futrell, J. Chem. Phys., in press.
[16] T. Yalcin, I.G. Csizmadia, M.R. Peterson, A.G. Harrison, J. Am. Soc. Mass Spectrom. 7 (1996) 233.

[17] M.J. Nold, C. Wesdemiotis, T. Yalcin, A.G. Harrison, Int. J. Mass Spectrom. Ion Processes 164 (1997) 137.
[18] C.F. Rodriquez, T. Shoeib, I.K. Chu, K.W.M. Siu, A.C. Hopkinson, J. Phys. Chem. A 104 (2000) 5335.
[19] G.A. Reid, R.J. Simpson, R.A.J. O'Hair, Int. J. Mass Spectrom. 190/191 (1999) 209.
[20] K. Vékey, Á. Somogyi, V.H. Wysocki, Rapid Commun. Mass Spectrom. 10 (1996) 911.
[21] M.J. Nold, B.A. Cerda, C. Wesdemiotis, J. Am. Soc. Mass Spectrom. 10 (1999) 1.
[22] B. Paizs, S. Suhai, Rapid Commun. Mass Spectrom. 15 (2001) 651.